Experimental Study on New Tool Holder Design to Reduce Vibration in Turning Operations

Eymen Akdeniz[1] · Hakan Arslan[2]

Abstract

Objectives To introduce and evaluate the performance of a novel tool holder design for turning operations on a CNC lathe. The study aimed to address the pervasive challenge of vibration in turning operations, which influences tool wear and the quality of the final surface finish.

Methods The experimental assessment involved comparing the new tool holder with a conventional steel one under varying cutting parameters, including feed rate, cutting speed, and depth of cut. A computer numerical control (CNC) lathe was utilized for the experiments. An analysis of variance (ANOVA) was employed to dissect the impacts of different cutting parameters on both vibration levels and surface roughness.

Results The experimental results highlighted significant advantages offered by the new tool holder. It achieved a remarkable reduction in vibration levels, ranging between 25.4 and 48.7% compared to the steel tool holder. Additionally, the new tool holder led to a noticeable improvement in surface roughness, with a reduction in the range of 21.5 to 31.5%. The ANOVA analysis underscored the depth of cut as the most influential parameter, with a paramount effect on both vibration amplitude and surface roughness.

Conclusions The research strongly recommends the adoption of the new tool holder, particularly in scenarios requiring extended overhangs. The innovative design demonstrated superior performance in reducing vibrations and improving surface roughness during turning operations. Furthermore, the study explored the application of shape memory alloys in turning cutting tools, emphasizing their substantial role in vibration reduction.

Keywords Turning · Tool holder · Vibration · Surface roughness · ANOVA analysis

Introduction

Vibrations are a common issue in machining operations, significantly impacting the quality of the manufacturing process, particularly the surface finish of the workpiece. These vibrations arise from the deformation of the workpiece during metal cutting processes such as turning, boring, drilling, and milling. Cutting operations can induce vibrations either through forced vibrations resulting from cutting forces or by chatter, which arises from dynamic interactions between the workpiece and the cutting tool. Chatter, also known as self-excited vibration, detrimentally affects the quality of the machined surface. To address these challenges, extensive research efforts have been made in the literature to mitigate vibrations during turning operations. These studies can be categorized into two main approaches: The first approach focuses on reducing vibrations in the cutting tool by adjusting cutting parameters. Researchers often employ Stability Lobe Diagrams (SLD) to identify stable and unstable regions by plotting critical cutting parameters against spindle speed. SLD diagrams are instrumental in maximizing material removal rates under stable cutting conditions [1]. By modifying cutting parameters like depth of cut, spindle speed, and cutting speed based on SLD diagrams, researchers can effectively prevent chatter during cutting operations [2–4]. Some scholars have even studied on expanding the stability boundaries of SLD diagrams. For example, Wang and Li [5] improved the weakest component of the machine structure, which was found to be the spindle, to alter the

✉ Eymen Akdeniz
  eymenakdeniz82@gmail.com

1 Sinerji Arms and Ammunition R&D Center,
  71450 Kırıkkale, Türkiye

2 Faculty of Engineering and Architecture, Kırıkkale
  University, Kırıkkale, Türkiye

dynamic behavior of the machining tool and achieve a higher stability limit in the SLD diagram. Recently, Qiu and Ge [6] introduced an enhanced method for predicting chatter vibration in turning using a width-distance lobe instead of a width-speed lobe. This method offers improved predictability and ease of use. However, it's important to note that relying on SLD diagrams may not be effective when high productivity is required. The second approach in the literature for mitigating vibration in machining processes involves the use of various types of dampers, categorized as passive, semi-active, and active damping techniques. Passive damping techniques enhance damping without requiring an external power source to dissipate vibration energy. Examples of passive dampers include friction dampers [7, 8], impact dampers [9], and tuned mass dampers (TMD) [10, 11]. In boring operations, for instance, chatter can be suppressed by employing a passive damper made of Cartridge brass (30% Zn and 70% Cu) attached to the tool holder [12]. Active damping methods use sensors to monitor vibrations and actuators to actively suppress these vibrations in real-time during machining [13]. Common technologies in active damping systems include piezoelectric and electromagnetic actuators [14, 15]. Semi-active dampers are passive devices that can be tuned in real-time but cannot generate damping forces themselves. Typically, semi-active dampers rely on the magneto-rheological (MR) damping effect to mitigate chatter in milling operations [16–18]. These two main approaches, adjusting cutting parameters and utilizing dampers, offer effective strategies for addressing the challenge of vibrations in machining processes, allowing for improved surface quality and manufacturing efficiency.

Numerous experimental investigations employing statistical approaches have been conducted to assess the impact of cutting parameters on both tool vibration and workpiece surface roughness during turning operations on diverse materials. Günay and Yücel, for instance, employed a Taguchi L18 orthogonal array to identify the optimal surface roughness conditions when machining high alloy cast iron with two varying hardness levels. The S/N (signal-to-noise) ratio was used, following the 'least is best' principle, to determine the ideal cutting conditions. Their findings indicated that, for workpieces with a hardness of 62 HRC, the feed rate exerted the most significant influence on surface roughness, while cutting speed was the primary factor for workpieces with a hardness of 50 HRC [19]. Rao and Venkatasubbaiah investigated into the effects of cutting parameters on surface roughness while turning AA7075 steel workpieces. Employing a Taguchi L9 orthogonal array and ANOVA analysis, they identified that feed rate and cutting speed were the most crucial factors affecting surface roughness. The optimal combination of cutting parameters for achieving low surface roughness was determined to be a cutting speed of 1000 m/min, a feed rate of 0.2 mm/rev, and a depth of cut

of 0.5 mm [20]. Salvi et al. investigated surface roughness in hard turning operations using the Taguchi method and highlighted that feed rate, followed by cutting speed, played a pivotal role in achieving low surface roughness [21]. Debnath et al. explored the effects of cutting fluid conditions and cutting parameters on surface roughness and tool wear during turning. Their research identified that the optimum cutting conditions for desired surface roughness and tool wear included high cutting speed, medium depth of cut, low feed rate, and high coolant flow speed [22]. Nalbant et al. studied the influence of optimal cutting parameters on surface roughness during the turning of AISI 1030 steel. They determined that the cutter nose radius, feed rate, and depth of cut were the most significant factors affecting surface roughness [23]. Cetin et al. conducted ANOVA analysis to investigate the impact of cutting parameters on cutting force and surface roughness during the turning of AISI 304L steel. Their results revealed high R-squared values (> 0.98) for surface roughness and shear force, with feed rate and depth of cut proving more influential than cutting speed and cutting fluids in enhancing surface quality and reducing cutting forces [24]. In a separate study, Bagaber and Yusoff optimized cutting parameters to minimize power consumption during dry turning of AISI 316 stainless steel. They found that the lowest cutting speed, highest feed rate, and greatest depth of cut yielded the minimum power consumption [25]. Likewise, Bhattacharya et al. investigated the effect of cutting parameters on surface roughness and power consumption in high-speed machining of AISI 1045 steel. Their research highlighted the significant impact of cutting speed on both surface roughness and power consumption, with other cutting parameters playing a relatively minor role [26].

Generally, metals and polymers are employed for vibration damping due to their viscoelastic characteristics. The damping capacity of these materials is notably influenced by their microstructure [27]. Recent studies have introduced methods to reduce vibrations during turning operations by incorporating materials with damping attributes into the tool holder. These materials include carbon fiber [28], polyurethane, nitride-butadiene rubber, butyl rubber [29], and foamed aluminum [30]. In the case of Shape Memory Alloys (SMAs), a significant amount of hysteresis between the loading and unloading phases results in the dissipation of a substantial portion of strain energy as heat. This dissipation imparts a damping function to SMAs, endowing them with exceptional damping capabilities [31].

In literature, shape memory alloys are usually used for vibration control in construction and civil engineering. However, this paper seeks to demonstrate their effectiveness in reducing vibrations during internal turning operations with a boring bar. It was created a novel boring bar model by combining SMAs and carbide materials, building on our previous research. Our prior work extensively analyzed this

innovative model through numerical and analytical methods. In this study, it was planned to further our research by conducting experiments using CNC turning techniques. These experiments will involve our newly developed SMA-infused boring bar, with results carefully compared to those from a standard steel boring bar. This research aims to explore new applications for SMAs in machining and vibration reduction, potentially extending their use beyond traditional engineering fields.

Material and Methods

The Developed Tool Holder

In Fig. 1, it can be observed the model that was formulated in a prior investigation produced by Akdeniz E. This study aimed to enhance the damping capability of the tool holder through the implementation of a negative damping mechanism. This mechanism involved the incorporation of a material possessing high damping capacity, namely foamed aluminum, within the tool holder's structure to effectively dissipate vibration energy [32]. The model comprises a tool holder constructed from TiNi3 alloy and features four carbide plates strategically positioned on each of its four sides. In the center of this tool holder assembly, there are three

cores, consisting of two carbide cores with a foamed aluminum core situated between them.

The mechanical properties of the different materials used in the structure of the tool holder are shown in Table 1.

Experimental Study

The experimental setup comprises several components, including a CNC lathe, computer, connection block, signal conditioner, Data Acquisition (DAQ) card, and a vibration measurement sensor, as illustrated in Fig. 2. In this experimental study, it was utilized the National Instruments brand BNC-2110 connection block, which serves as the transmitter between the signal conditioner and the accelerometer. The signal conditioner establishes the connection between the connection block and the computer's DAQ card. Within the signal conditioner, electrical signals originating from the accelerometer undergo conversion

Table 1 Mechanical properties of the used materials

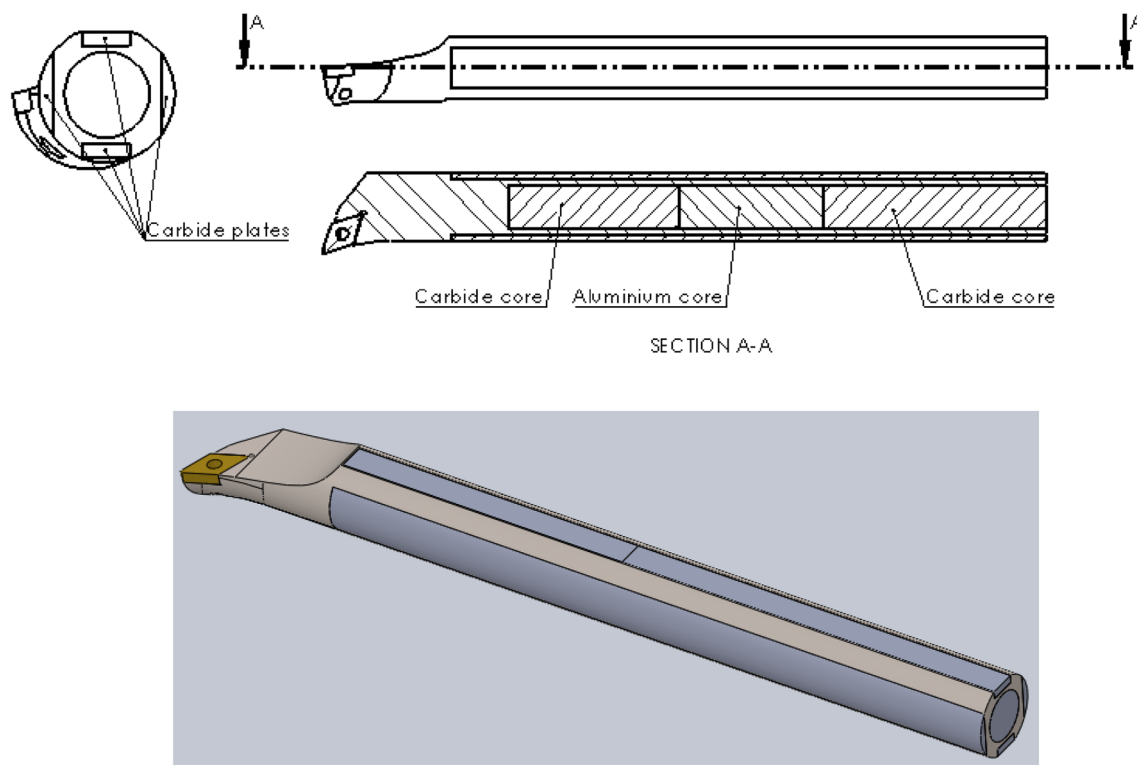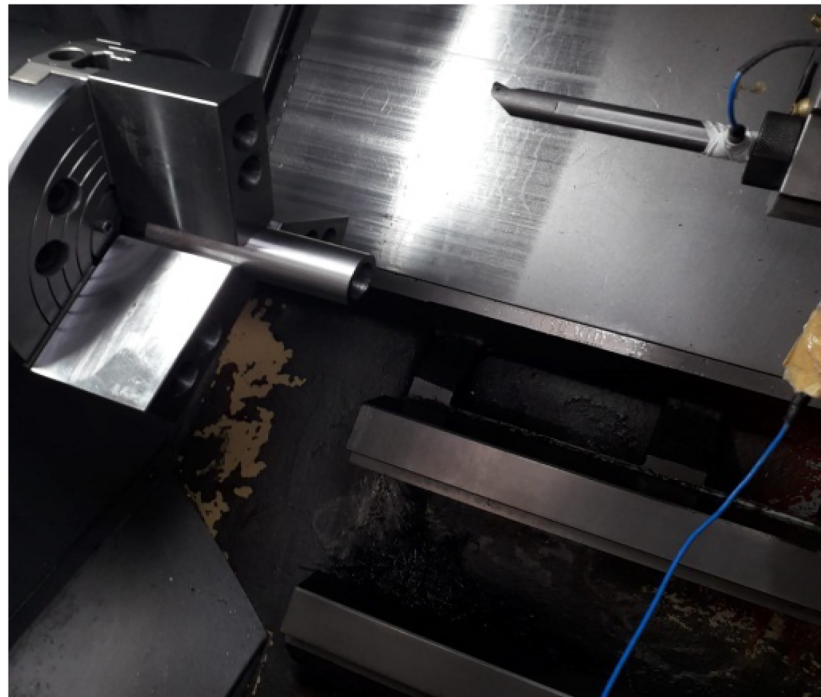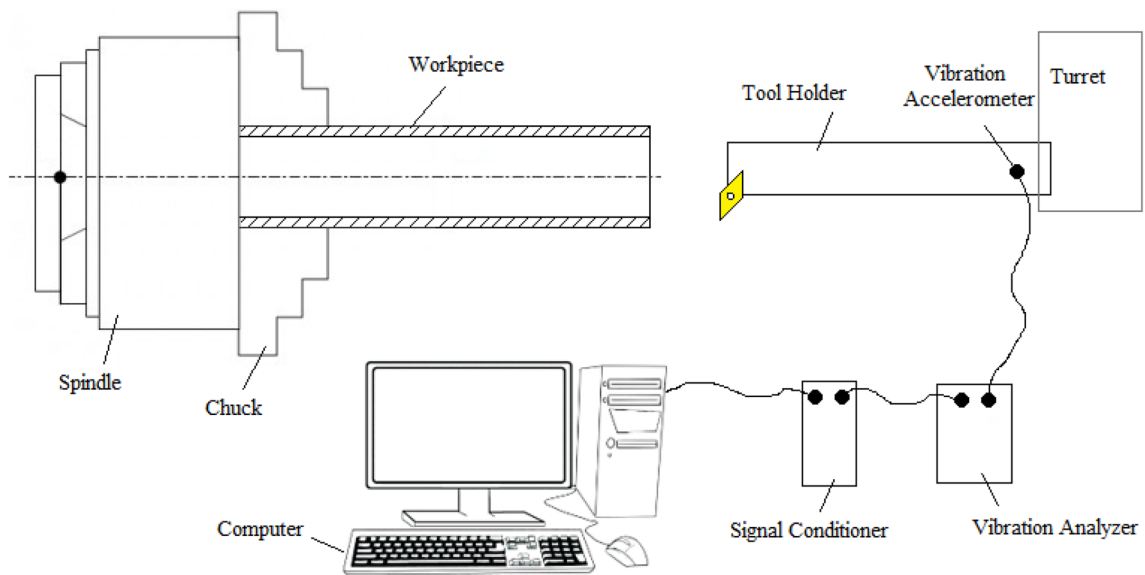| Mechanical Properties	TiNi3 Alloy	Carbide
Density (kg/m^3)	7960	14,550
Young Modulus (Pa)	2.51×10^{11}	6×10^{11}
Poisson's Ratio	0.28	0.3

Fig. 1 The proposed tool holder in the previous study [32]

(a)

(b)

Fig. 2 **a** Photo of CNC Lathe **b** Schematic Representation of Experimental System

and filtering to become a portable voltage signal (analog signal). For the experiments, PCB 482 A16 was employed as a signal conditioner. The DAQ card facilitates the transfer of data acquired from the vibration sensor to the computer environment and was connected to the computer's main board, utilizing the National Instruments brand PCI M series 6281 DAQ card.

The gathering of vibrations during turning operations was conducted using the Matlab 2010 program. Figure 3 displays both the newly proposed tool holder and the
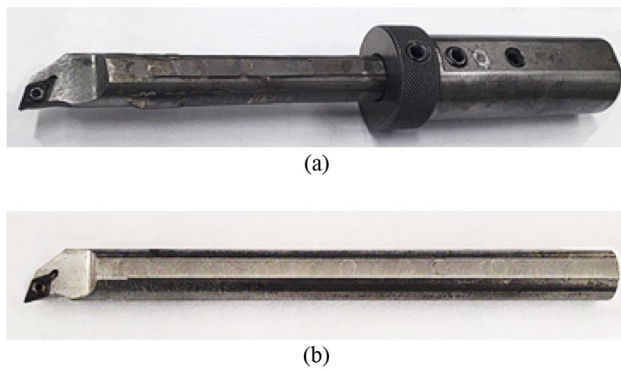
(a)

(b)

Fig. 3 Tool holders used in experiments. **a** Proposed new tool holder, **b** Normal tool holder

Table 2 Cutting Parameters for Experiments

Experiment No	Cutting speed (rpm)	Feed rate (mm/rev)	Depth of cut (mm)
E1	300	0,1	0,2
E2	300	0,15	0,4
E3	300	0,2	0,6
E4	500	0,1	0,4
E5	500	0,15	0,6
E6	500	0,2	0,2
E7	700	0,1	0,6
E8	700	0,15	0,2
E9	700	0,2	0,4

commercially available steel tool holder utilized in the experiments. The experiments involved three key cutting parameters: cutting speed, feed rate, and depth of cut, with their respective values provided in Table 2. These values were determined according to the Taguchi L9 method. The tool holder had an overhang length of 120 mm. For the workpiece material, a 1060 steel tube with dimensions of Ø23 X Ø32 X 140 mm (Fig. 4) was employed. Additionally, DCMT 070204-HMP carbide inserts were utilized throughout the experiments. Surface roughness of the machined samples was assessed using a Mitutoyo SJ-210 device.

During the experimental phase, a secondary recording of vibrations was conducted, varying the cutting parameters. Following each experiment, the surface roughness was measured, and photographs of the workpiece surface were captured. Each experiment employed a distinct workpiece to ensure independent measurements.
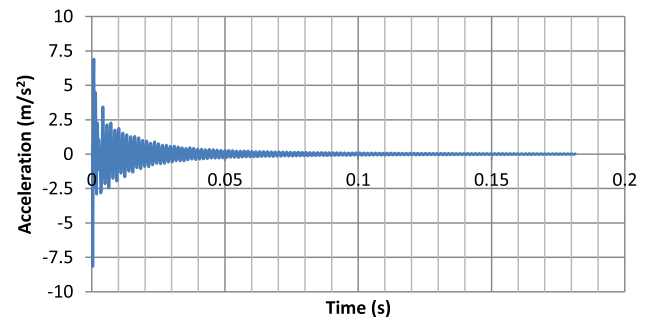

Fig. 4 Workpiece

**Fig. 5** Acceleration-time graph (modal test)

Results and Discussion

Experimental Modal Test

Before executing the experiments, a modal test was conducted using a hammer and an accelerometer to identify the natural frequency of the cutting tool. This test yielded an acceleration-time graph, depicted in Fig. 5, and a Fast Fourier Transform (FFT) graph of the acceleration amplitude-frequency spectrum was generated as well (Fig. 6). The modal test served the purpose of pinpointing the machine's first natural frequency and resonance characteristics. This precaution ensured that the experimental parameters chosen did not match with the machine's resonance frequencies. The exclusive consideration of the system's first natural frequency is due to its association with the critical cutting speed, making the machining system prone to chatter. Furthermore, the first natural frequency is essential for evaluating the dynamic stability of the machining process. As observed in Fig. 6, the first natural frequency of the machine was determined to be 664 Hz.

The Vibration RMS Values and FFT Graphs

The Root Mean Square (RMS) is calculated as the square root of the mean square, which itself is the average of

Fig. 6 FFT graph for modal test
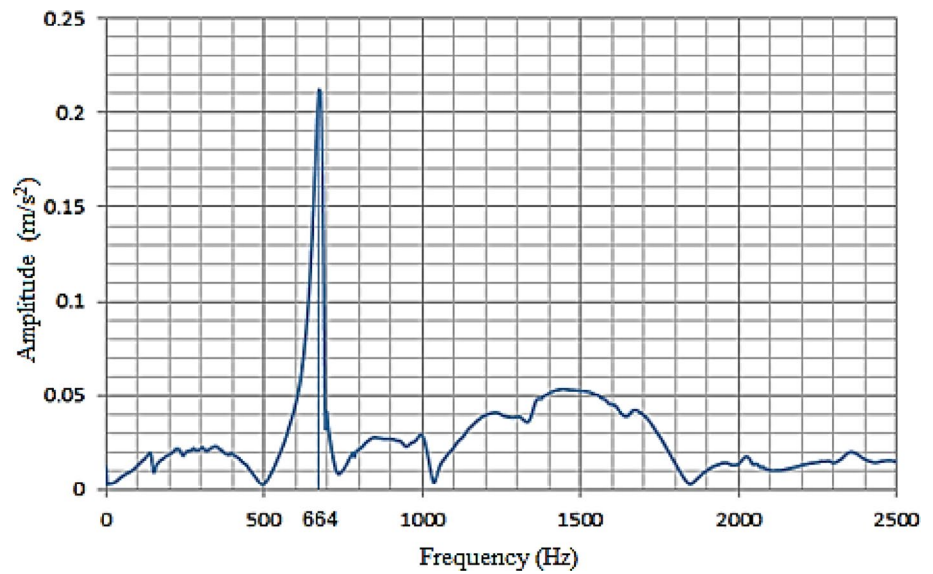
Table 3 Acceleration-Time RMS values

Experiment No	Steel tool holder	New tool holder	Vibration reduction rate
E1	0,50	0,34	32%
E2	0,82	0,57	30.5%
E3	1,19	0,80	32.7%
E4	0,8	0,41	48.7%
E5	1,56	0,90	42.3%
E6	0,45	0,32	28.9%
E7	0,56	0,41	26.8%
E8	0,55	0,41	25.4%
E9	1,91	1,02	46.6%

the squares of numerical values. In vibration analysis, the RMS metric serves as a tool to compare two signals, helping determine which one possesses larger amplitude of vibration. A higher RMS value in a signal signifies a greater amplitude of vibration. Table 3 displays the RMS values obtained from the acceleration-time graphs for all the experiments conducted.

Based on the findings from the experiments, the utilization of the newly proposed tool holder resulted in a notable reduction in vibrations, ranging from 25 to 48%. An examination of the RMS values and the vibration reduction ratios indicates that the recommended application for the proposed tool holder is in scenarios involving high cutting speeds and substantial depths of cut. This is attributed to the significant reduction in vibration achieved at these specific values. To conduct an in-depth analysis, Fig. 7 exhibits frequency spectrum graphs (FFT graphs) illustrating the acceleration-time data for all experiments carried

out using both the conventional steel tool holder and the new tool holder.

Resonance, characterized by maximum amplitudes, tends to manifest at frequencies in close proximity to the machine's natural frequency, as established during the modal test, which recorded a value of 664 Hz. Upon inspecting Fig. 7, it becomes evident that during experiment 1, the peak amplitude of vibration for the conventional steel boring bar occurred at a frequency of 688 Hz, while the peak amplitude for the new bar was observed at a frequency of 654 Hz. Furthermore, the spectrum reveals that the vibration amplitudes for the steel boring bar are notably greater compared to those for the new tool holder. In experiment 2, the peak amplitude of vibration for the conventional steel boring bar appeared at a frequency of 703 Hz, whereas for the new tool holder, it appeared at a frequency of 698 Hz. Once again, the vibration amplitudes for the steel boring bar surpass those for the new one. In experiment 3, the peak amplitude for the steel boring bar was noted at 698 Hz, while for the new tool holder, it occurred at 649 Hz. In experiment 4, the peak vibration amplitude for the steel boring bar was recorded at 712 Hz, whereas for the new tool holder, it appeared at 683 Hz. Here, too, it's evident that the peak amplitude of the spectrum for the steel boring bar is substantially higher than that for the new one.

In experiment 5, the peak amplitude of vibration for the steel boring bar surfaced at a frequency of 654 Hz, whereas for the new tool holder, it emerged at 712 Hz. Remarkably, the vibration amplitudes in the spectra for the two tool holders closely resemble each other. Meanwhile, in experiment 6, the peak vibration amplitude for the steel boring bar was observed at a frequency of 678 Hz, while for the new tool holder, it manifested at 654 Hz. For experiment 7, the peak vibration amplitude for the steel boring bar was identified at
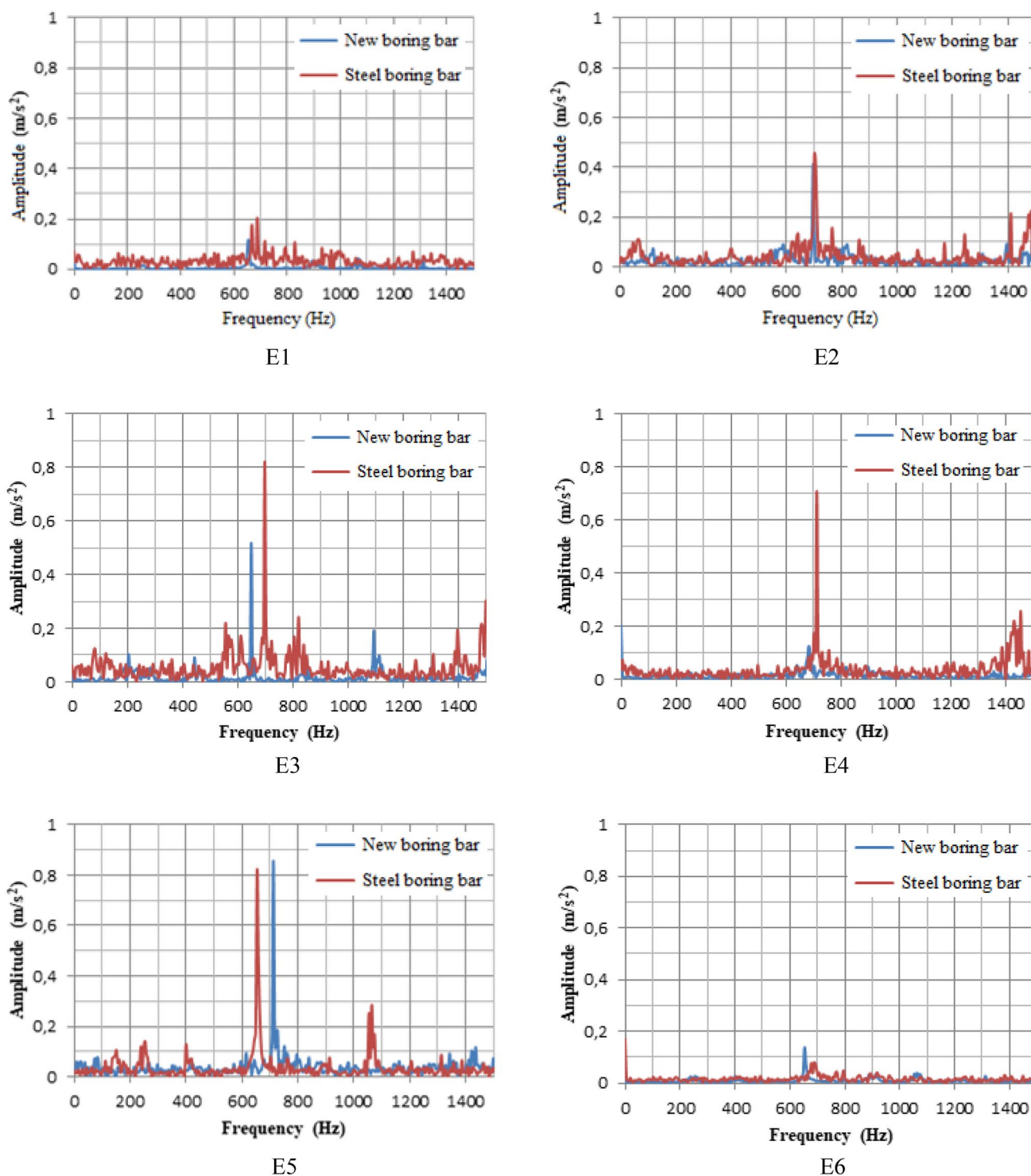
Fig. 7 Comparison between Amplitude-Frequency spectrum graphs for steel and new tool holder for all experiments (E1 to E9)

659 Hz, whereas for the new tool holder, it was observed at 664 Hz. Notably, in experiments 5, 6 and 7, the peak amplitude in the spectrum for the new tool holder exceeded that of the steel bar, although the overall vibration amplitudes for the steel bar remained greater. In these experiments, there is a possibility that the new tool holder might experience effects near to resonance at its first natural frequency, particularly considering the cutting parameters applied in these experimental conditions. This resonance results in the amplification of vibrations.
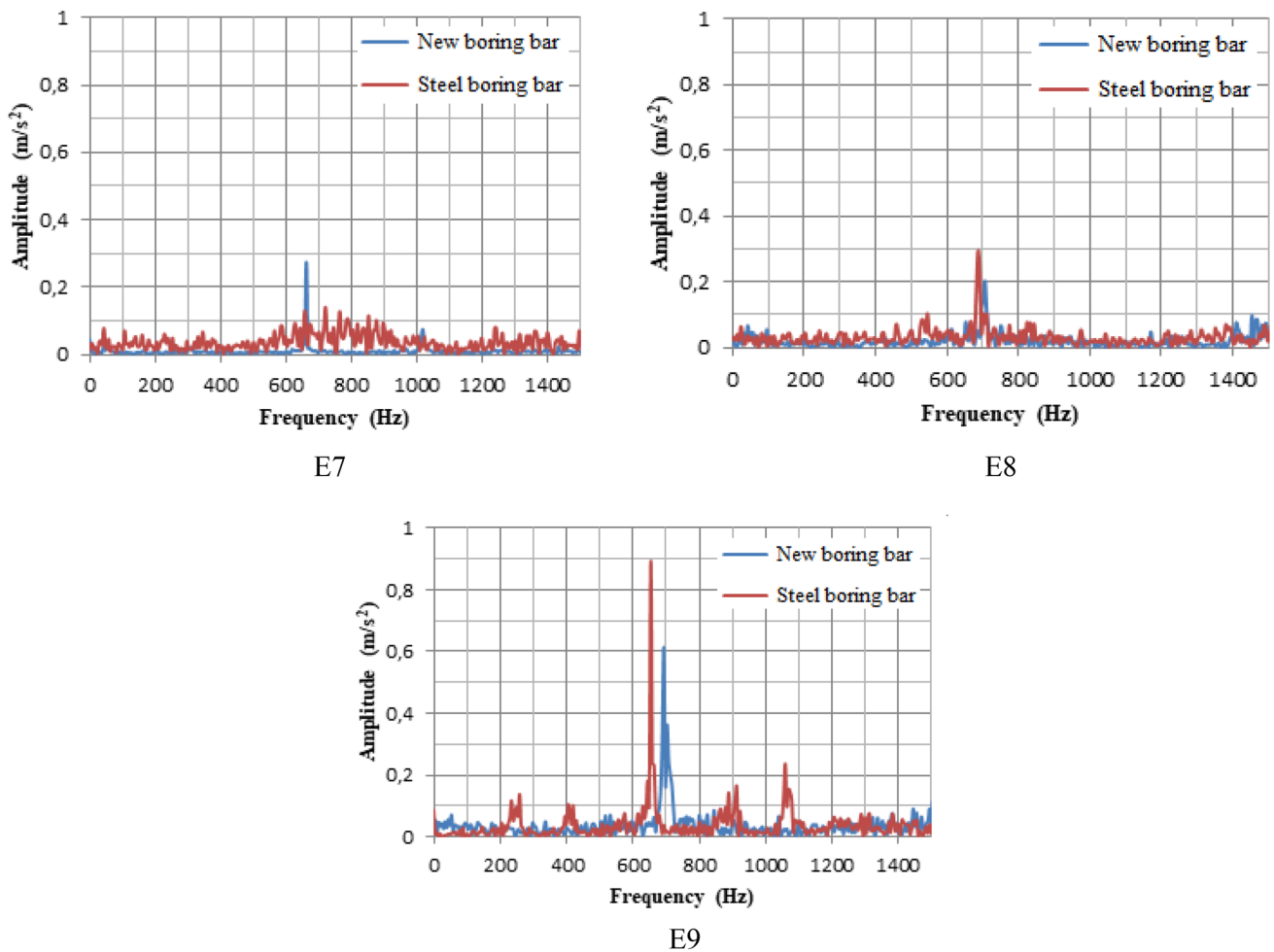
Springer

E7

E8

E9

Fig. 7 (continued)

In experiment 8, the peak vibration amplitude for the steel boring bar occurred at a frequency of 688 Hz, while for the new tool holder, it appeared at 708 Hz. In experiment 9, the peak vibration amplitude for the steel boring bar materialized at a frequency of 658 Hz, whereas for the new tool holder, it was noted at 693 Hz. Throughout experiments 8 and 9, the peak amplitude in the spectrum for the steel boring bar exceeded those for the new tool holder. Notably, the lowest amplitude vibrations were observed in experiment 6, characterized by high feed rates and low depths of cut. Conversely, the highest amplitude vibrations were encountered in experiment 5, which involved high depths of cut, and in experiment 9, where cutting speeds were high.

Power Spectral Density (PSD) Graphs

When considering FFT graphs for both the steel and the new tool holder, variations can occur when adjusting the frequency range due to the random nature of cutting tool vibrations in turning operations. To effectively compare vibrations between these two tool holders, a more robust tool is required. The primary advantage of utilizing power spectral density (PSD) against FFT for analyzing random vibrations is that it normalizes the amplitude values relative to the frequency band. This normalization eliminates the dependence on bandwidth, enabling a fair comparison of vibration levels throughout different lengths.

The PSD of a signal provides an overview of the signal's power distributed throughout various frequencies. Elevated PSD levels within a frequency range indicate the presence of chatter during cutting operations compared to stable cutting. As depicted in Fig. 8, the PSD plots of vibration signals for both the new tool holder and the steel one throughout all experiments illustrate that the PSD level for the conventional steel boring bar exceeds that of the new tool holder. This discrepancy signifies greater vibration in the steel bar.

Furthermore, in order to compare the two signals, the RMS values of the PSD graphs for both the steel and the new tool holder were computed and presented in Table 4. It becomes evident from these RMS values that,
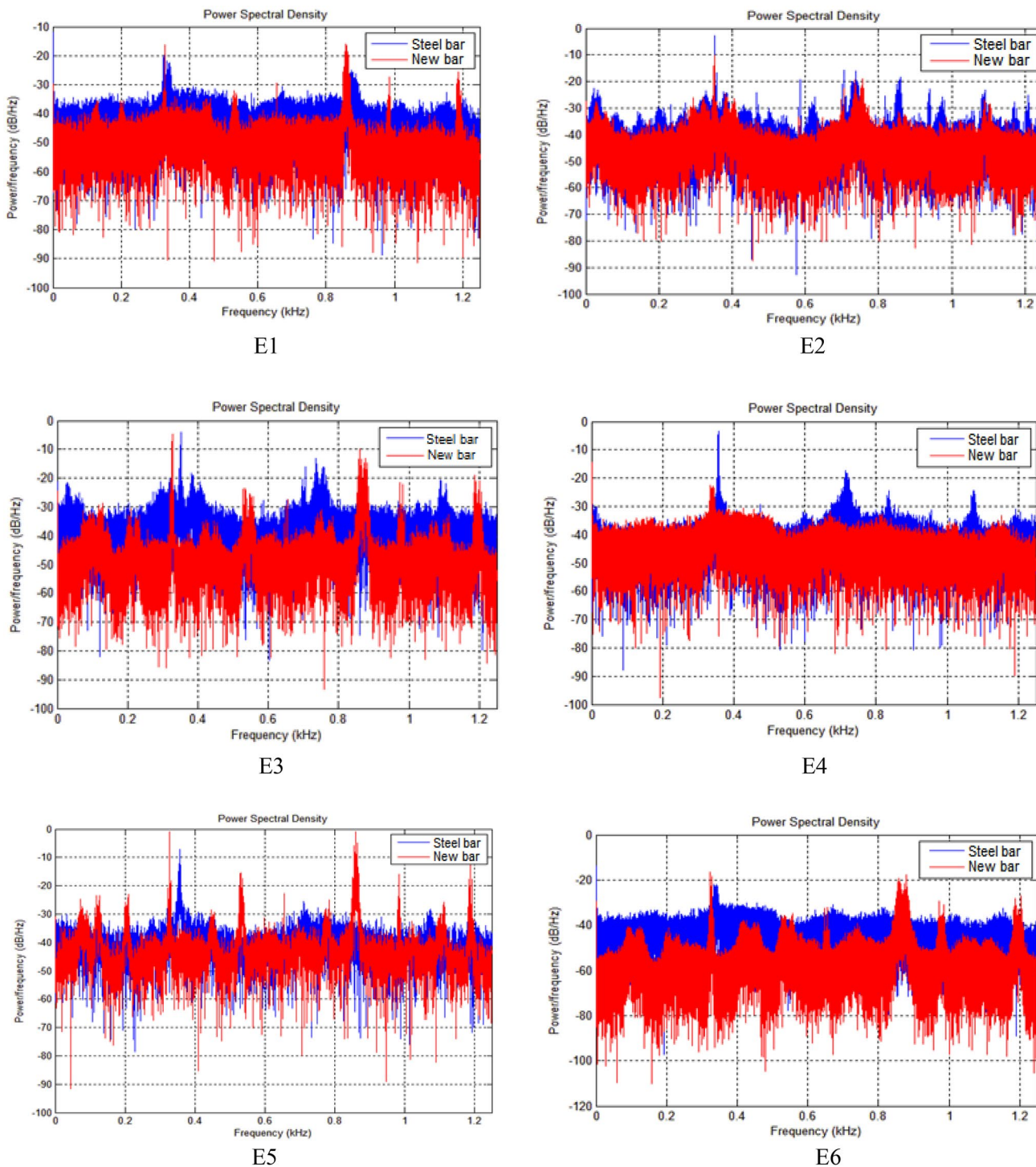
Fig. 8 Comparison between PSD graphs for steel and new tool holder for all experiments (E1 to E9)

throughout all experiments, the PSD levels for the steel tool holder consistently exceeded those for the new tool holder. This discrepancy underscores that the vibration of the conventional steel boring bar surpasses that of the new tool holder. The variance in RMS values between the steel boring bar and the new tool holder ranges from 4.37% to 18.87%. The highest difference ratio was observed in experiment 3, while the lowest difference ratio was noted in experiment 9.
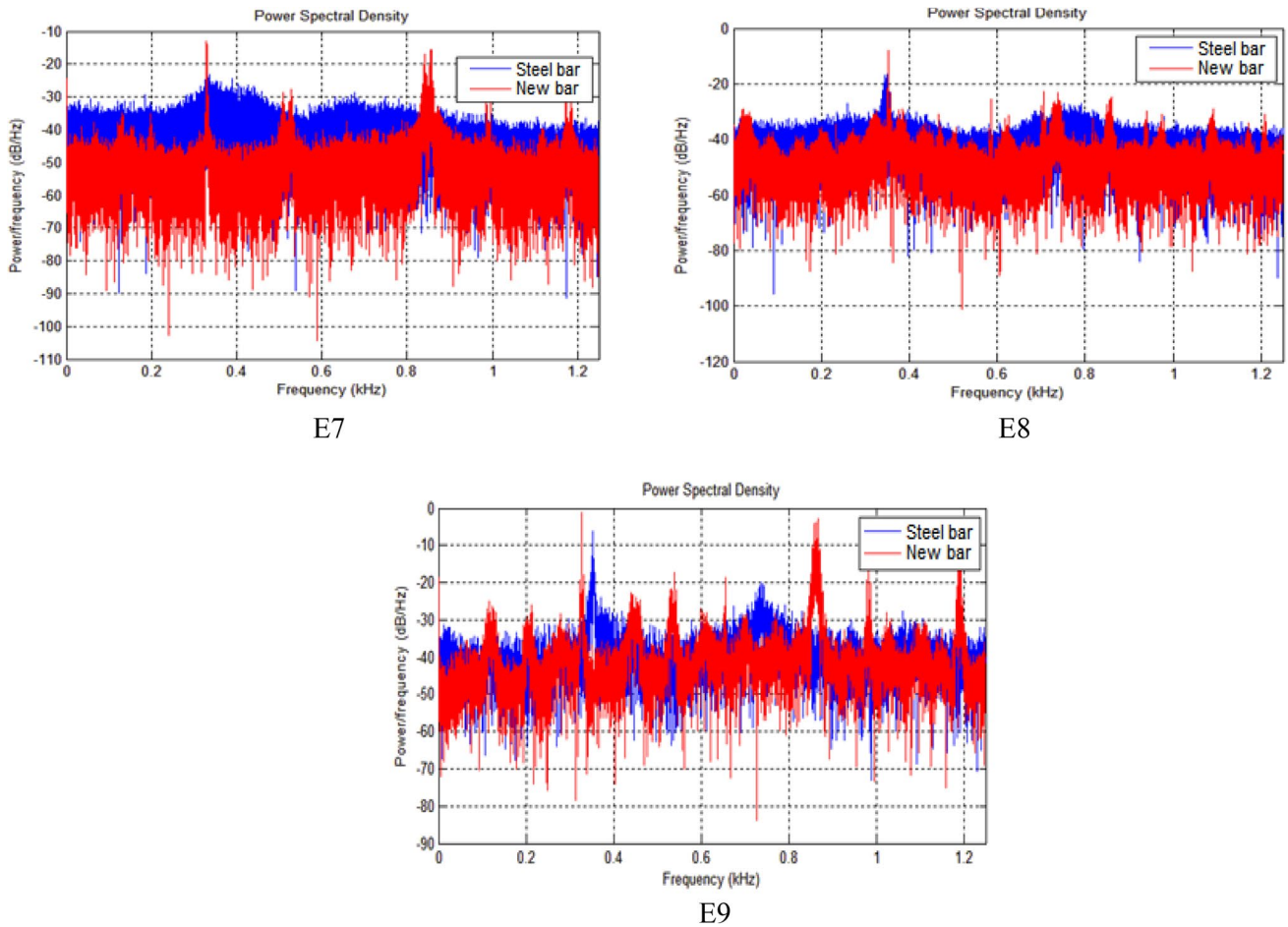
E7

E8

E9

Fig. 8 (continued)

Table 4 RMS values of the PSD graphs

Experiment No	RMS values		
	Steel bar	New bar	Difference %
E1	41,57	38,33	7,79%
E2	42,37	39,48	6,82%
E3	45,62	37,01	18,87%
E4	45,32	40,31	11,05%
E5	44,91	41,26	8,13%
E6	55,15	48	12,96%
E7	51,41	46,77	9,03%
E8	46,25	40,49	12,45%
E9	39,55	37,82	4,37%

Table 5 Surface roughness values

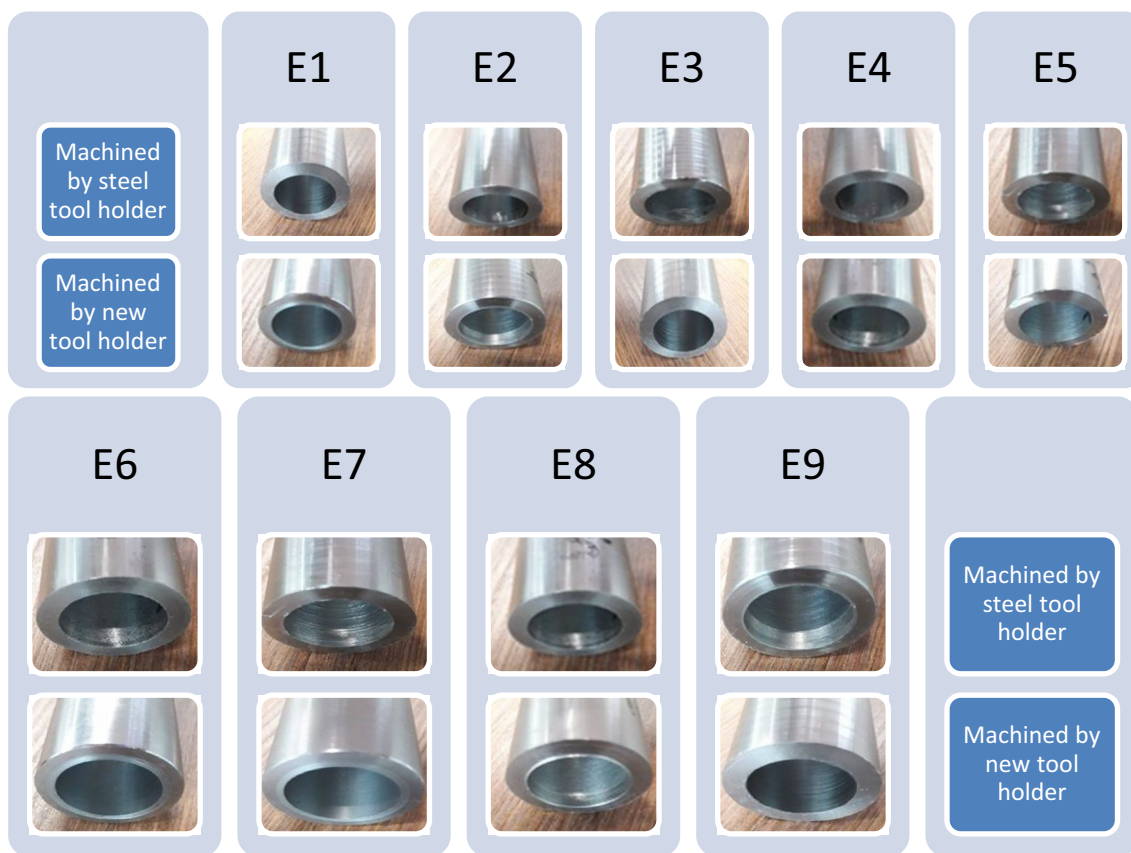| Experiment No	Steel tool holder	New tool holder	Surface roughness reduction %
E1	2.20	1.58	28.4%
E2	1.34	1.05	21,5%
E3	1.72	1.24	27.6%
E4	1.49	1.18	20.9%
E5	1.62	1.19	26.4%
E6	3.88	2.77	28.6%
E7	2.02	1.45	28.3%
E8	3.13	2.56	18.4%
E9	2.76	1.89	31.5%

Surface Roughness

The surface roughness of the internal machined surfaces of the workpieces was assessed throughout all experiments using a Mitutoyo SJ-210 device. The resulting surface roughness values (Ra) for the machined surfaces are presented in Table 5.

The decrease in surface roughness on the workpieces ranges from 21.5% to 31.5%. Table 6 highlights a substantial improvement in the surface roughness of the

Table 6 Machined workpieces

machined workpieces when employing the new tool holder, with experiments E6, E7, and E9 particularly exhibiting significant improvements.

ANOVA Analysis

To investigate the impact of cutting parameters on both vibration amplitude and workpiece surface roughness, an ANOVA analysis was conducted using Minitab software. The Signal/Noise ratio graphs, depicting the results obtained
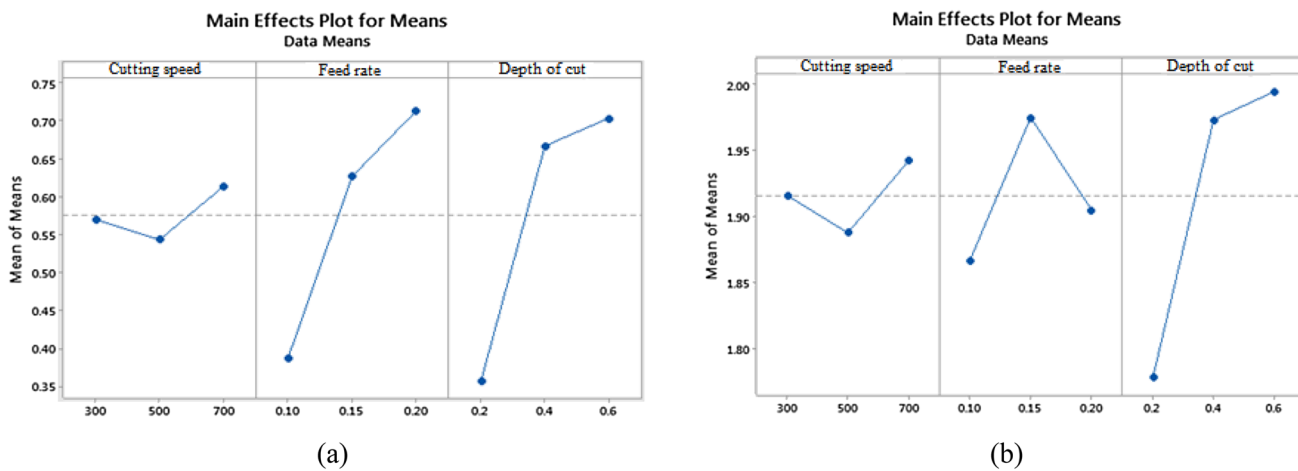

Fig. 9 Signal-to-noise ratio for: **a** vibration amplitude **b** surface roughness of new tool holder

Analysis of Variance

Source	DF	Contribution	F-Value	P-Value
Cutting speed	2	3.62%	1.98	0.336
Feed rate	2	39.26%	21.49	0.044
Depth of cut	2	55.29%	30.27	0.032
Error	2	1.83%		
Total	8	100.00%		

Model Summary

S	R-sq	R-sq(adj)
0.0404145	98.17%	92.69%

(a)

Analysis of Variance

Source	DF	Contribution	F-Value	P-Value
Cutting speed	2	5.93%	3.49	0.223
Feed rate	2	31.61%	18.60	0.051
Depth of cut	2	60.76%	35.75	0.027
Error	2	1.70%		
Total	8	100.00%		

Model Summary

S	R-sq	R-sq(adj)
0.0378432	98.30%	93.20%

(b)

Fig. 10 ANOVA results depending on **a** vibration amplitude **b** surface roughness

for both vibration amplitude and surface roughness, are presented in Fig. 9.

This figure reveals that, based on the Signal/Noise ratio analysis, the optimal values for vibration amplitude correspond to the following cutting parameters: a cutting speed of 500 rpm, a feed rate of 0.1 mm/rev, and a depth of cut of 0.2 mm. Similarly, for achieving lower surface roughness, the ideal cutting parameters are a cutting speed of 500 rpm, a feed rate of 0.1 mm/rev, and a depth of cut of 0.2 mm.

As depicted in the ANOVA results illustrated in Fig. 10, the depth of cut exerts the most significant influence, accounting for 55.29% of the variance in vibration amplitude, followed by the feed rate at 39.26%, while the cutting speed has the least impact at 3.62%. The experiments exhibit a high level of reliability, with a rate of 98.17%.

Additionally, the results highlight that the depth of cut is the predominant factor affecting surface roughness, contributing to 60.76% of the variance. The feed rate also plays a substantial role, with an effective rate of 31.61% on surface roughness, whereas the cutting speed exerts the least influence, with a rate of 5.93%. The reliability of the experiments remains high at 98.3%.

Conclusion

This research endeavor was built upon a previously published study by the authors to verify the effectiveness of the proposed new tool holder experimentally. The proposed innovative tool holder design harnessed the unique damping characteristics of shape memory alloys, the resilience of foamed aluminum material, and the precision of high-density carbide components. The conducted experiments encompassed a comprehensive assessment, comparing the performance of the newly introduced cutting tool holder with that of a conventional steel cutting tool holder. It was focused on two critical aspects: an in-depth vibration analysis and a meticulous evaluation of the surface roughness of the machined workpieces. The results of the experiments yielded compelling benefits associated with the use of the new tool holder. Specifically, it delivered a noteworthy reduction in cutting tool vibrations, achieving an impressive amplitude decrease ranging from 25.4% to 48.7%. Furthermore, it significantly improved the surface quality of the machined pieces, enhancing it by a percentage ranging from 21.5% to 31.5% when compared to the commercial steel tool holder. Furthermore, ANOVA analysis shed light on the depth of cut as the most influential parameter impacting both the vibration amplitude of the cutting tool and the surface roughness of the machined workpiece. In contrast, cutting speed emerged as the parameter with the least impact. Using the new tool holder is strongly recommended, particularly in scenarios demanding extended overhangs. This article introduces the utilization of shape memory alloys in the manufacturing of turning cutting tools, emphasizing their substantial role in reducing vibrations during operation.

In future studies, the performance of the new boring bar can be investigated for a range of workpiece materials, such as aluminum or copper. Moreover, exploring the use of shape memory alloy to reduce vibrations in cutting tools during milling operations is also worth considering.

Authorship Contributions EA: Methodology, experimental investigation, data optimization, writing. HA: Conceptualization, supervision, validation, formal analysis, review & editing.

References

1. Großmann K, Löser M (2013) Synthesis of stability lobe diagrams. In: Denkena B, Hollmann F (eds) Process machine

interactions. Lecture notes in production engineering. Springer, Berlin

2. Abele E, Fiedler U (2004) Creating stability lobe diagrams during milling. CIRP Ann 53(1):309–312. https://doi.org/10.1016/S0007-8506(07)60704-5

3. Quintana G, Ciurana J, Teixidor D (2008) A new experimental methodology for identification of stability lobes diagram in milling operations. Int J Mach Tools Manuf 48(15):1637–1645

4. Galdino dos Santos R, Teixeira Coelho R (2014) A contribution to improve the accuracy of chatter prediction in machine tools using the stability lobe diagram. J. Manuf. Sci. Eng. 136(2):21005. https://doi.org/10.1115/1.4025514

5. Wang J, Lee K (1996) Suppression of chatter vibration of a CNC machine centre—an example. Mech Syst Signal Processing 10:551–560. https://doi.org/10.1006/mssp.1996.0038

6. Qiu J, Ge R (2018) An improved stability lobe and turning chatter characteristic investigation. Int J Mechanic Sci 149:338–348. https://doi.org/10.1016/j.ijmecsci.2018.10.006

7. Edhi E, Hoshi T (2001) Stabilization of High Frequency Chatter Vibration in Fine Boring by Friction Damper. J Int Soc Precis Eng Nanotechnol 25:224–234. https://doi.org/10.1016/S0141-6359(01)00074-5

8. Ziegert JC, Stanislaus C, Schmitz TL (2006) Enhanced Damping in Long Slender Endmills. J Manuf Process 8:32–46. https://doi.org/10.1016/S1526-6125(06)70100-1

9. Ema S, Marui E (2000) Suppression of Chatter Vibration of Boring Tools Using Impact Dampers. Int J Mach Tools Manuf 40:1141–1156. https://doi.org/10.1016/S0890-6955(99)00119-4

10. Hahn RS (1951) Design of Lanchester Damper for Elimination of Metal Cutting Chatter. Journal of Engineering for Industry 73(3):331–335

11. Hayati S, Hajaliakbari M, Rajabi Y et al (2018) Chatter reduction in slender tool holder via a tunable holder with variable mass and stiffness. Journal of Engineering Manufacture 232(12):2098–2108. https://doi.org/10.1177/0954405417690554

12. Prasannavenkadesan V, Elango A, Chockalingam S (2015) Chatter Suppression in Boring Process Using Passive Damper, International Journal of Aerospace and Mechanical. Engineering 9(11):1932–1936

13. A. Preumont, Vibration Control of Active Structures, Springer, 1997.

14. Neugebauer R, Denkena B, Wegener K (2007) Mechatronic Systems for Machine Tools. CIRP Ann 56(2):657–686. https://doi.org/10.1016/j.cirp.2007.10.007

15. Sims ND, Bayly PV, Young KA (2005) Piezoelectric Sensors & Actuators for Milling Tool Stability Lobes. J Sound Vib 281(3–5):743–762. https://doi.org/10.1016/j.jsv.2004.02.014

16. Ahmed GMS, Reddy PR, Seetharamaiah N (2012) Experimental Investigation of Magneto Rheological Damping Effect on Surface Roughness of Work Piece during End Milling Process. Int J Precis Eng Manuf 13(6):835–844. https://doi.org/10.1007/s12541-012-0109-0

17. Sam Paul, P., Varadarajan, A.S., Ajay Vasanth, X. et al. Effect of magnetic field on damping ability of magnetorheological damper during hard turning. Archiv.Civ.Mech.Eng 14, 433–443 (2014). https://doi.org/10.1016/j.acme.2013.11.001

18. Suhas S. Aralikatti, Hemantha Kumar, Tool vibration isolation in hard turning process with magnetorheological fluid damper, Journal of Manufacturing Processes, Volume 88, 2023, Pages 202–219, ISSN 1526–6125, https://doi.org/10.1016/j.jmapro.2023.01.044.

19. Günay M, Yücel E (2013) Application of Taguchi method for determining optimum surface roughness in turning of high-alloy white cast iron. Measurement 46(2):913–919. https://doi.org/10.1016/j.measurement.2012.10.013

20. Rao CM, Venkatasubbaiah K, Babu SP, Srinivas C (2016) Optimization of surface roughness in CNC turning using Taguchi method and ANOVA, International Journal of Advanced. Science and Technology 93:1–14. https://doi.org/10.14257/ijast.2016.93.01

21. Salvi SB, Deshmukh RR, Deshmukh SD (2013) Analysis of surface roughness in hard turning by using Taguchi method. Int J Eng Sci Technol 5(02):365–370

22. Debnath S, Reddy MM, Yi QS (2016) Influence of cutting fluid conditions and cutting parameters on surface roughness and tool wear in turning process using Taguchi method. Measurement 78:111–119. https://doi.org/10.1016/j.measurement.2015.09.011

23. Nalbant M, Gökkaya H, Sur G (2007) Application of Taguchi method in the optimization of cutting parameters for surface roughness in turning. Mater Des 28(4):1379–1385. https://doi.org/10.1016/j.matdes.2006.01.008

24. Cetin MH, Ozcelik B, Kuram E, Demirbas E (2011) Evaluation of vegetable based cutting fluids with extreme pressure and cutting parameters in turning of AISI 304L by Taguchi method. J Clean Prod 19(17–18):2049–2056. https://doi.org/10.1016/j.jclepro.2011.07.013

25. Bagaber SA, Yusoff AR (2017) Multi-objective optimization of cutting parameters to minimize power consumption in dry turning of stainless steel 316. J Clean Prod 157:30–46. https://doi.org/10.1016/j.jclepro.2017.03.231

26. Bhattacharya A, Das S, Majumder P, Batish A (2009) Estimating the effect of cutting parameters on surface finish and power consumption during high speed machining of AISI 1045 steel using Taguchi design and ANOVA. Prod Eng Res Devel 3(1):31–40. https://doi.org/10.1007/s11740-008-0132-2

27. de Batist R (1983) High damping materials: Mechanisms and applications. J Phys 44(C9):C9–C39

28. Thorenz B, Friedrich M, Westermann HH et al (2019) Evaluation of the influence of different inner cores on the dynamic behavior of boring bars. Proc CIRP 81:1171–1176

29. Liu Y, Liu Z, Song Q et al (2019) Analysis and implementation of chatter frequency dependent constrained layer damping tool holder for stability improvement in turning process. J Mater Process Technol 266:687–695

30. Song Q, Shi J, Liu Z et al (2016) Boring bar with constrained layer damper for improving process stability. Int J Adv Manuf Technol 83:1951–1966

31. Chung DDL (2001) A review: Materials for vibration damping. J Mater Sci 36:5733–5737

32. E. Akdeniz H. Arslan, A new design of tool holder using TiNi3 alloy to reduce vibration in turning operations, Proceedings of the Institution of Mechanical Engineers, Part B: Journal of Engineering Manufacture, 237(1–2) (2023) 105–121, https://doi.org/10.1177/09544054221104607.